Based on the Nonlinear State Equations of 6-DOF Robot with Application to Autonomous Flight

Zhou Hongcheng(✉) and Fang Yuzhuo

School of Electronic and Information Engineering, Jinling Institute of Technology, Nanjing 211169, China
945516882@qq.com

Abstract. The paper provides a linearized model of the quad rotor aircraft. Linearization is carried out around each state to optimize the system for larger flight envelopes. Each coupling term is represented by fixing and changing each time one state. Non-fragile optimal controller realization for the quad rotor aircraft is obtained by considering two different approaches for computation of controller fragility, stability radii comparison and weighted eigenvalue sensitivity calculation. A numerical method for reduction of controller fragility is presented. The simulation results show that the time delay compensation effect is well realized.

Keywords: Linearization · Non-fragile optimal · Controller · Nyquist · Circle criterion

1 Introduction

The derived nonlinear translational and rotational model, quad rotor aircraft needs to be simplified for control design [1]. The drag and rolling moment caused by speed are ignored, and the thrust and drag coefficients are assumed to be constant,

$$\begin{aligned} T_i &= b\Omega_i^2 \\ Q_i &= d\Omega_i^2 \end{aligned} \tag{1}$$

In this context, b and d represent the thrust factor and resistance factor, respectively, for a quad rotor aircraft system. The system's inputs consist of a vertical force input denoted as u_1, roll actuator input as u_2, pitch actuator input as u_3, and yaw moment input as u_4, given by [2],

The inputs for a quad rotor aircraft system can be represented as follows: the vertical force input is designated as u_1, the roll input as u_2, the pitch input as u_3, and the yaw

X. Chen et al. (Eds.): IoTaaS 2023, LNICST 585, pp. 152–162, 2025.
https://doi.org/10.1007/978-3-031-70507-6_13

input as u_4. These particular inputs are defined by the equation provided below:

$$\left.\begin{aligned} u_1 &= b(\Omega_1^2 + \Omega_2^2 + \Omega_3^2 + \Omega_4^2) \\ u_2 &= b(\Omega_4^2 - \Omega_2^2) \\ u_3 &= b(\Omega_3^2 - \Omega_1^2) \\ u_4 &= d(\Omega_2^2 + \Omega_4^2 - \Omega_1^2 - \Omega_3^2) \end{aligned}\right\} \tag{2}$$

Therefore, the 6-DOF nonlinear equation for controlling a quad rotor aircraft can be formulated in state space representation. $\dot{\mathbf{X}} = f(\mathbf{X}, \mathbf{u})$ using input vectors $\mathbf{u}$ and state vectors $\mathbf{X}$. The state is defined as [3],

$$\left.\begin{aligned} x_1 = x \quad x_2 = \dot{x} \\ x_3 = y \quad x_4 = \dot{y} \\ x_5 = z \quad x_6 = \dot{z} \\ x_7 = \phi \quad x_8 = \dot{\phi} \\ x_9 = \theta \quad x_1 = \dot{\theta} \\ x_{11} = \psi \; x_1 = \dot{\psi} \end{aligned}\right\} \tag{3}$$

The state vector X is represented by,

$$\mathbf{X} = \left[x\ \dot{x}\ y\ \dot{y}\ z\ \dot{z}\ \phi\ \dot{\phi}\ \theta\ \dot{\theta}\ \psi\ \dot{\psi} \right] \tag{4}$$

The transformation matrix between the rate of change in orientation angles $\left(\dot{\varphi}, \dot{\theta}, \dot{\psi}\right)$ and the angular velocity (p, q, r) of an object can be considered as [4]. Simulation results have shown that this assumption is valid. Thus,

$$\left(\dot{\phi}, \dot{\theta}, \dot{\psi}\right) \approx (p, q, r) \tag{5}$$

Provided a translation model for a quad rotor aircraft that meets the real-time constraints of the embedded control loops, is given by [5],

$$f(\mathbf{X}, \mathbf{u})_{translational} = \begin{pmatrix} \dot{x} \frac{(\cos\phi \sin\theta \cos\psi + \sin\phi \sin\psi)}{m} u_1 \\ \dot{y} \ \frac{(\cos\phi \sin\theta \sin\psi - \sin\phi \cos\psi)}{m} u_1 \\ \dot{z} \ -g + \frac{(\cos\phi \cos\theta)}{m} u_1 \end{pmatrix} \tag{6}$$

2 Linearization of Nonlinear State Equations

Equations (6) are nonlinear and must be linearized in order to design linear controllers [6]. The linear state space is represented as,

$$\mathbf{A} = \begin{bmatrix} 0\,1\,0\,0\,0\,0\,0 & 0 & 0 & 0 & 0 & 0 \\ 0\,0\,0\,0\,0\,0\,0 & 0 & 0 & 0 & 0 & 0 \\ 0\,0\,0\,1\,0\,0\,0 & 0 & 0 & 0 & 0 & 0 \\ 0\,0\,0\,0\,0\,0\,0 & 0 & 0 & 0 & 0 & 0 \\ 0\,0\,0\,0\,0\,1\,0 & 0 & 0 & 0 & 0 & 0 \\ 0\,0\,0\,0\,0\,0\,0 & 0 & 0 & 0 & 0 & 0 \\ 0\,0\,0\,0\,0\,0\,0 & 1 & 0 & 0 & 0 & 0 \\ 0\,0\,0\,0\,0\,0\,0 & 0 & 0\ \dot{\psi}_e\left(\frac{J_y - J_z}{J_x}\right) & 0 & \dot{\theta}_e\left(\frac{J_y - J_z}{J_x}\right) \\ 0\,0\,0\,0\,0\,0\,0 & 0 & 0 & 1 & 0 & 0 \\ 0\,0\,0\,0\,0\,0\,0\ \dot{\psi}_e\left(\frac{J_z - J_x}{J_y}\right) & 0 & 0 & 0 & \dot{\varphi}_e\left(\frac{J_z - J_x}{J_y}\right) \\ 0\,0\,0\,0\,0\,0\,0 & 0 & 0 & 0 & 0 & 1 \\ 0\,0\,0\,0\,0\,0\,0\ \dot{\theta}_e\left(\frac{J_x - J_y}{J_z}\right) & 0\ \dot{\varphi}_e\left(\frac{J_x - J_y}{J_z}\right) & 0 & 0 \end{bmatrix} \begin{bmatrix} x \\ \dot{x} \\ y \\ \dot{y} \\ z \\ \dot{z} \\ \phi \\ \dot{\varphi} \\ \theta \\ \dot{\theta} \\ \psi \\ \dot{\psi} \end{bmatrix} \tag{7}$$

$$\mathbf{B} = \begin{bmatrix} 0 & 0 & 0 & 0 \\ \frac{\cos\phi \sin\theta \cos\psi + \sin\phi \sin\psi}{m} & 0 & 0 & 0 \\ 0 & 0 & 0 & 0 \\ \frac{\cos\phi \sin\theta \cos\psi - \sin\phi \sin\psi}{m} & 0 & 0 & 0 \\ 0 & 0 & 0 & 0 \\ \frac{\cos\phi \cos\theta}{m} & 0 & 0 & 0 \\ 0 & 0 & 0 & 0 \\ 0 & \frac{l}{J_x} & 0 & 0 \\ 0 & 0 & 0 & 0 \\ 0 & 0 & \frac{l}{J_y} & 0 \\ 0 & 0 & 0 & 0 \\ 0 & 0 & 0 & \frac{1}{J_z} \end{bmatrix} \begin{bmatrix} u_1 \\ u_2 \\ u_3 \\ u_4 \end{bmatrix} \tag{8}$$

3 Controllability and Observability

The non-controllable and non-observable states of the state-space model, which are not connected to any input or output, are eliminated [7]. The resulting state space model is structurally minimal. After eliminating non-minimum state dynamics, we only have left

the rotating subsystem, given by

$$\mathbf{A}\dot{\mathbf{X}} + \mathbf{B}\mathbf{U} = \begin{bmatrix} 0 & 1 & 0 & 0 & 0 & 0 \\ 0 & 0 & 0 & \dot{\psi}_e\left(\frac{J_y - J_z}{J_x}\right) & 0 & \dot{\theta}_e\left(\frac{J_y - J_z}{J_x}\right) \\ 0 & 0 & 0 & 1 & 0 & 0 \\ 0 & \dot{\psi}_e\left(\frac{J_z - J_x}{J_y}\right) & 0 & 0 & 0 & \dot{\varphi}_e\left(\frac{J_z - J_x}{J_y}\right) \\ 0 & 0 & 0 & 0 & 0 & 1 \\ 0 & \dot{\theta}_e\left(\frac{J_x - J_y}{J_z}\right) & 0 & \dot{\varphi}_e\left(\frac{J_x - J_y}{J_z}\right) & 0 & 0 \end{bmatrix} \begin{bmatrix} \phi \\ \dot{\varphi} \\ \theta \\ \dot{\theta} \\ \psi \\ \dot{\psi} \end{bmatrix} + \begin{bmatrix} 0 & 0 & 0 & 0 \\ 0 & \frac{l}{J_x} & 0 & 0 \\ 0 & 0 & 0 & 0 \\ 0 & 0 & \frac{l}{J_y} & 0 \\ 0 & 0 & 0 & 0 \\ 0 & 0 & 0 & \frac{1}{J_z} \end{bmatrix} \begin{bmatrix} u_1 \\ u_2 \\ u_3 \\ u_4 \end{bmatrix} \tag{9}$$

To account for the lack of direct coupling between the input and output of the system, the direct conversion matrix, denoted as D, is assigned a value of zero. This indicates that there is no direct correlation or interaction between the input variables and the output variables within the system [8].

3.1 System Implementation

Let the transfer function be expressed as,

$$G(\overline{\theta}) = \frac{b(\overline{\theta})}{a(\overline{\theta})} = \frac{\sum_{i=0}^{n_b} b_i \overline{\theta}^i}{\sum_{i=0}^{n_a} a_i \overline{\theta}^i} \tag{10}$$

where, n_b and n_a are the numerator and denominator respectively, such that $n_a > n_b$ [9].

Where, n_b and n_a represent the numerator and denominator respectively, with the constraint that $n_a > n_b$ [9].

Let controller (proper) be defined as,

$$H(\overline{\theta}) = \frac{q(\overline{\theta})}{p(\overline{\theta})} = \frac{\sum_{i=0}^{n_q} q_i \overline{\theta}^i}{\sum_{i=0}^{n_p - 1} p_i \overline{\theta}^i + \overline{\theta}^{n_p}} \tag{11}$$

where, n_q and n_p represent the numerator and denominator of the controller respectively, such that $n_p \geq n_q$.

3.2 Stability Radius & Weighted Eigenvalue Sensitivity

Radius of stability ball can be considered as one of the measures for fragility. If the parameterization $\mathbf{X}$ undergoes perturbation, the measure of stability radius r_s is determined by,

$$r_s := \{\inf[\|\Delta\|] : \text{closed } \textit{loop system is} \text{ in stability}\} \tag{12}$$

Another measure for fragility is weighted eigenvalue sensitivity Ψ_{total} defined as,

$$\Psi_{total} = \sum_{k=1}^{N} w_k \Psi_k \tag{13}$$

where N represents the number of closed-loop eigenvalues, w_k is a non-negative real weighting factor, and Ψ_k denotes the weighted sum of the 2-norm sensitivity of an individual closed-loop system eigenvalue to perturbations in the controller parameters. This is calculated using the following equation [10]

$$\Psi_k = \sum_{i=1}^{n_x} \left(\frac{\partial \lambda_k}{\partial x_i} \right)^2 \tag{14}$$

4 Application to 3-DOF Rotorcraft

The optimal (non-fragile) controller realization method is applied to a standard control problem, i.e., longitudinal pitch hold controller of a 3-DOF UH-60 rotorcraft. Consider the longitudinal dynamics of a hovering UH-60 rotorcraft. At hover, the vertical and longitudinal dynamics are decoupled. In Fig. 1, the standard block diagram correctly describes the rotorcraft.

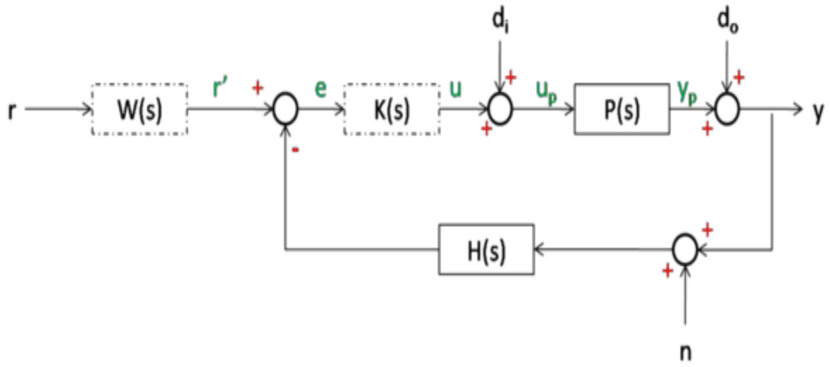

Fig. 1. Block Diagram of the rotor aircraft system

The dynamics of the aircraft in the longitudinal direction around the hover state are influenced by factors such as horizontal velocity, pitch attitude, and periodic pitch control. In particular, the horizontal velocity is characterized by the model described in [11],

$$\frac{\dot{x}}{B_{lc}} = X_{Blc} \left[\frac{s^2 - M_q s - \frac{gM_{Blc}}{X_{Blc}}}{s^3 - (X_u + M_q)s^2 + M_q X_u s + gM_u)} \right] \tag{15}$$

The pitch attitude of the aircraft is influenced by various factors such as horizontal speed denoted by $\dot{x}$ in $ft/$ sec, and periodic pitch control denoted by B_{lc} in degrees. The pitch attitude can be described as follows:

$$\frac{\theta}{B_{lc}} = M_{Blc} \left[\frac{s + \left(\frac{X_{Blc} M_u}{M_{Blc}} - X_u \right)}{s^3 + (X_u + M_q)s^2 + M_q X_u s + gM_u} \right] \tag{16}$$

where θ is the pitch attitude in *deg*.

Figure 2 shows the block diagram for this controller [12].

$$B_{lc} = \frac{[K_\theta]}{s}\left(\theta_c - \left[\frac{50^2(s+b)^2}{(s+50)^2 b^2}\right]\theta\right) \tag{17}$$

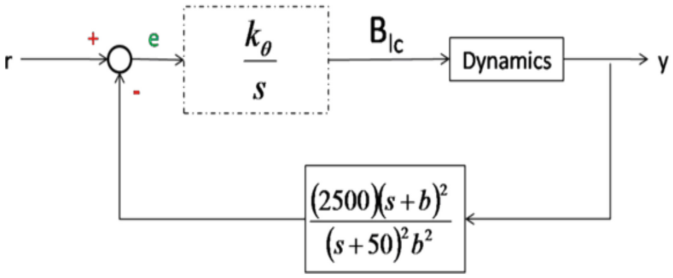

Fig. 2. U-60 rotorcraft Longitudinal Pitch-Hold

The pitch attitude of the aircraft is influenced by several variables: θ represents the true pitch attitude in radians, θ_c represents the commanded pitch in radians, b represents the control design parameter, and $k_\theta \leq 0$ represents the proportional gain constant for the pitch attitude. After the step command, the desirable low-frequency pitch attitude command is represented by $b = 2.0$ and $k_\theta = -1$.

Therefore, using a transfer function form controller, the calculated weighted eigenvalues 1.6011×10^{10} have extremely high sensitivity, while the actual stability radius is 1.000×10^{-3}. In the normalized form of modal state space, the controller is characterized by the weighted eigenvalue sensitivity denoted as 2.3021×10^{3} and the real stability radius denoted as 42.23×10^{-3}. The optimal weighted eigenvalue sensitivity is represented by 214.3169, while the actual stable radius is denoted as 59.18×10^{-3}. Hence, for this particular application, the weighted closed-loop eigenvalue sensitivity serves as a reasonable measure of controller vulnerability.

4.1 Open Loop Controller Performance

The implementation of the controller was simulated in an open loop using a discrete time controller. Different canonical forms, namely adjoint form, modal form, optimal form, and equilibrium form, were obtained. The response of the open-loop controller was compared with the response of the Simulink discrete time state space block under the same conditions. To excite the controller in the open loop, a Chirp signal with a frequency range of 0.1 Hz–10 Hz was used. Random signal inputs were also utilized to confirm the results obtained from the Chirp signal.

From Fig. 3, Upon analysis, it is evident that among open loop systems, the optimal non-fragile form demonstrates the most favorable outcomes. Following this, the balanced implementation and modal form exhibit relatively lower performance, respectively.

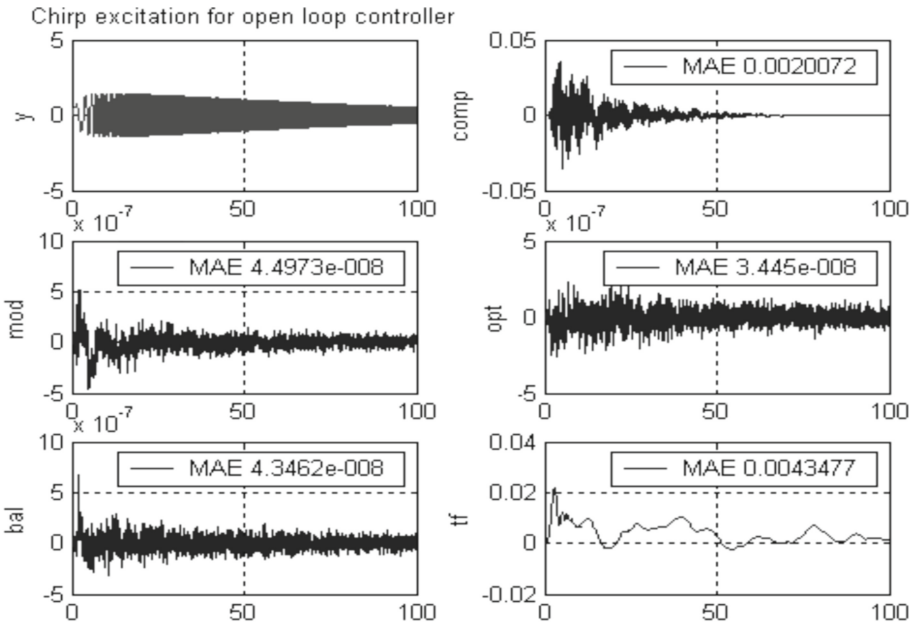

Fig. 3. The output response in different normative forms

4.2 Closed Loop Performance

The comparison results are presented in Fig. 4. The obtained results clearly demonstrate that the optimal form of the closed-loop system yields the most optimal outcome, followed by the balanced implementation and modal form.

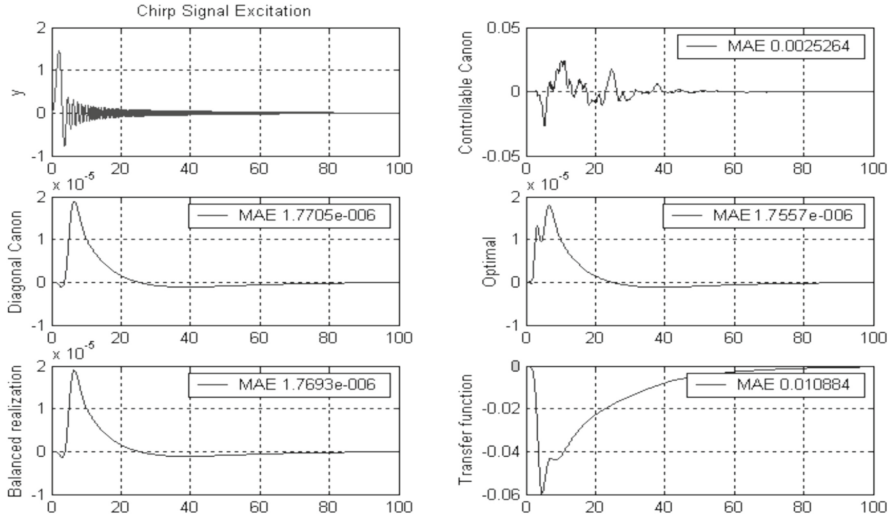

Fig.4. The output response in different normative forms

An effective method for reducing controller vulnerability has been derived. This method applies complex Schur decomposition and QR decomposition to obtain suboptimal solutions. The method is applied to longitudinal pitch attitude controller of a UH-60 rotorcraft reducing its fragility by a large margin.

4.3 Non-fragile Optimal Control Design

When designing a control system, always choose the control vector **u** to minimize the system's performance indicators. For the design of linear quadratic regulators, the performance index J is given by the following equation:

$$J = \int_0^\infty \left(x'Qx + u'Ru\right)dt \tag{18}$$

In the given context, Q represents a positive definite matrix that can be either Hermite or real symmetric, while R represents a positive definite Hermite symmetric matrix. The variable u is unconstrained. The minimum performance index J of a state space system is defined using the minimum principle as follows,

$$\min_{u(t)} J = x\left(t_f\right)'\mathbf{S}\left(t_f\right)x\left(t_f\right) + \frac{1}{2}\int_{t_0}^{t_f}\left(x'Qx + u'Ru\right)dt \tag{19}$$

And assuming that $S\left(t_f\right) \geq 0, Q \geq 0, R \geq 0$. To determine the minimum value, the Hamiltonian function is formulated as follows:

$$H = \frac{1}{2}\left(x'Qx + u'Ru\right) + \lambda'(Ax + Bu) \tag{20}$$

And the following optimal conditions must be met:

$$\left[\frac{\partial H}{\partial u}\right]' = 0 \quad and \quad \left[\frac{\partial H}{\partial x}\right]' = -\dot{\lambda}(t) \tag{21}$$

Equation (21) gives, $u(t) = -R^{-1}B^T\dot{\lambda}(t)$, the optimal control is

$$\dot{\lambda} = -\left(Qx(t) + A'\lambda(t)\right) \tag{22}$$

The optimal control (22) is substituted into the state space system model to derive the resulting expression.

$$\begin{bmatrix}\dot{x}\\ \dot{\lambda}\end{bmatrix} = \begin{bmatrix}A & -BR^{-1}B'\\ -Q & -A'\end{bmatrix}\begin{bmatrix}x\\ \lambda\end{bmatrix} \triangleq H\begin{bmatrix}x\\ \lambda\end{bmatrix} \tag{23}$$

Equation (23) can be substituted,

$$\lambda = Px \tag{24}$$

Regarding the differential Eq. (24), we have

$$\frac{d\lambda}{dt} = \frac{dP}{dt}x + P\frac{dx}{dt} \tag{25}$$

Since $\dot{x} = dx/dt$ and $\dot{\lambda} = d\lambda/dt$, from the equation of state, we obtain

$$\begin{aligned} P\frac{dx}{dt} &= PAx - PBR^{-1}B'Px \\ \frac{d\lambda}{dt} &= -Qx - A'Px \end{aligned} \tag{26}$$

By substituting (25) in (26), we achieved the following differential equation,

$$-\frac{dP}{dt} = A'P + PA + Q - PBR^{-1}B'P \tag{27}$$

The state feedback gain matrix K is utilized to revise the control signal u,

$$u = -Kx,\ K = R^{-1}B'P \tag{28}$$

In order to get the state feedback gain matrix K, $dP\big/dt \to 0$, and the positive definite solution of the algebraic Riccati equation (ARE), an asymptotically stable closed-loop system was obtained. Then we write the state space equation of the quad rotor aircraft as,

To obtain the state feedback gain matrix K, $dP\big/dt \to 0$ as well as the positive definite solution of the algebraic Riccati equation (ARE), an asymptotically stable closed-loop system is established. This involves writing the state space equation for the quadrotor aircraft as follows:

$$\begin{aligned} \dot{x} &= (A - BK)x + Bu \\ y &= Cx \end{aligned} \tag{29}$$

Figure 5 illustrates the closed-loop diagram for the system using LQR state feedback gain A.

In order to ensure a meaningful optimization problem, it is required that Q be symmetric positive semidefinite and R be symmetric positive definite. Specifically, Q must be symmetric positive semidefinite to meet this requirement. Similarly, for meaningful optimization problems, R must be symmetric positive definite.

The parameters used for the simulation are,$l = 0.3\,m$,$J_x = 0.0158\ \text{kg} \cdot \text{m}^2$,$J_y = 0.0154\ \text{kg} \cdot \text{m}^2$, $J_z = 0.0309\ \text{kg} \cdot \text{m}^2$ and $m = 0.6\text{kg}$. The initial conditions used are $\varphi = \theta = \psi = 0.5$ rad, $\dot{\varphi} = \dot{\theta} = \dot{\psi} = 0.5$ rad/sec.

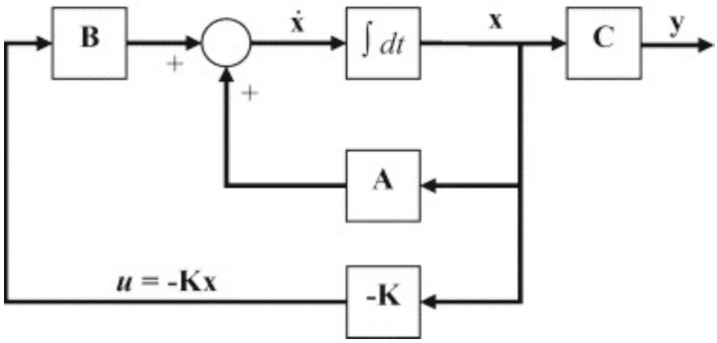

Fig. 5. Closed loop block diagram

5 Conclusions

An improved and efficient controller vulnerability reduction method was designed and implemented for a quad rotor craft that significantly reduces controller vulnerability. This method combines ordered complex Schur decomposition and QR decomposition to converge to suboptimal solutions. Various implementations of controllers for rotor craft were obtained and compared, including open-loop and closed-loop controllers. The Simulink state space block was utilized for this comparison, and the calculation of overall error was based on the Mean Absolute Error (MAE) parameter. The stability analysis of the non-fragile MIMO control system was conducted using extended Nyquist and Circle methods.

Acknowledgment. This work was supported by Cooperative Project of Jiangsu Province production, teaching and research (No. BY2021381), Jin Ling Institute of Technology Ph. D. Startup Fund(jit-b-202314).

References

1. Karahan, O., Karci, H.: Swarm intelligence based nonlinear friction and dynamic parameters identification for a 6-DOF robotic manipulator. J. Int. Robot. Syst. **108**(2), 19 (2023)
2. Sancak, K.V., Bayraktaroglu, Z.Y.: Nonlinear Computed Torque Control of 6-DoF Parallel Manipulators. Int. J. Control Automat. Syst. **20**(7), 2297–2311 (2022)
3. Cruz, G.L., Alazki, H., Cortes-Vega, D., et al.: Application of robust discontinuous control algorithm for a 5-DOF industrial robotic manipulator in real-time. J. Intell. Rob. Syst. **101**(4), 1–17 (2021)
4. Wang, H., Li, X., Liu, X., et al.: Fuzzy sliding mode active disturbance rejection control of an autonomous underwater vehicle-manipulator system. J. Ocean Univ. China **19**(5), 1081–1093 (2020)
5. Khankalantary, S., Badri, P., Mohammadkhani, H.: Designing a hierarchical model-predictive controller for tracking an unknown ground moving target using a 6-DOF quad-rotor. Int. J. Dyn. Control **9**, 985–999 (2021)

6. Sai, H., Xu, Z., Li, Y., et al.: Adaptive nonsingular fast terminal sliding mode impedance control for uncertainty robotic manipulators. Int. J. Precis. Eng. Manuf. **22**(12), 1947–1961 (2021)
7. Li, C., Ren, C., Ding, Y., et al.: Non-singular terminal sliding mode control of an omnidirectional mobile manipulator based on extended state observer. Int. J. Int. Robot. Appl. **5**(2), 219–234 (2021)
8. Loucif, F., Kechida, S., Sebbagh, A.: Whale optimizer algorithm to tune PID controller for the trajectory tracking control of robot manipulator. J. Braz. Soc. Mech. Sci. Eng. **42**(1), 1–11 (2020)
9. Kumar, J., Kumar, V., Rana, K.P.S.: Fractional-order self-tuned fuzzy PID controller for three-link robotic manipulator system. Neural Comput. Appl. **32**(11), 7235–7257 (2020)
10. Liu, A., Zhao, H., Song, T., et al.: Adaptive control of manipulator based on neural network. Neural Comput. Appl. **33**(9), 4077–4085 (2021)
11. Tran, D.T., Truong, H.V.A., Ahn, K.K.: Adaptive nonsingular fast terminal sliding mode control of robotic manipulator based neural network approach. Int. J. Precis. Eng. Manuf. **22**(3), 417–429 (2021)
12. Ma, F., Li, J., et al.: Tensor product based polytopic LPV system design of a 6-DoF multistrut platform. Int. J. Control. Autom. Syst.Autom. Syst. **20**(1), 137–146 (2022)